A theoretical multiscale treatment of protein-protein electron transfer: the ferredoxin/ferredoxin-NADP⁺ reductase and flavodoxin/ferredoxin-NADP⁺ reductase systems

Suwipa Saen-oon[1], Israel Cabeza de Vaca[1], Diego Masone[2], Milagros Medina[3] and Victor Guallar[1,4]

[1]*Joint BSC-CRG-IRB Research Program in Computational Biology, Barcelona Supercomputing Center, Jordi Girona 29, E-08034 Barcelona, Spain*
[2]*CONICET, Facultad de Ciencias Exactas y Naturales, Universidad Nacional de Cuyo, Padre Jorge Contreras 1300, Mendoza 5500, Argentina*
[3]*Department of Biochemistry and Molecular and Cellular Biology and Institute of Biocomputation and Physics of Complex Systems, University of Zaragoza, E-50009 Zaragoza, Spain*
[4] *Institució Catalana de Recerca i Estudis Avançats (ICREA), Passeig Lluís Companys 23, E-08010 Barcelona, Spain*

ABSTRACT

In the photosynthetic electron transfer (ET) chain, two electrons transfer from photosystem I to the flavin-dependent ferredoxin-NADP⁺ reductase (FNR) via two sequential independent ferredoxin (Fd) electron carriers. In some algae and cyanobacteria (as *Anabaena*), under low iron conditions, flavodoxin (Fld) replaces Fd as single electron carrier. Extensive mutational studies have characterized the protein-protein interaction in FNR/Fd and FNR/Fld complexes. Interestingly, even though Fd and Fld share the interaction site on FNR, individual residues on FNR do not participate to the same extent in the interaction with each of the protein partners, pointing to different electron transfer mechanisms. Despite of extensive mutational studies, only FNR/Fd X-ray structures from *Anabaena* and maize have been solved; structural data for FNR/Fld remains elusive. Here, we present a multiscale modelling approach including coarse-grained and all-atom protein-protein docking, the QM/MM e-pathway analysis and electronic coupling calculations, allowing for a molecular and electronic comprehensive analysis of the ET process in both complexes. Our results, consistent with experimental mutational data, reveal the ET in FNR/Fd proceeding through a bridge-mediated mechanism in a dominant protein-protein complex, where transfer of the electron is facilitated by Fd loop-residues 40-49. In FNR/Fld, however, we observe a direct transfer between redox cofactors and less complex specificity than in Fd; more than one orientation in the encounter complex can be efficient in ET.

KEYWORDS:

Protein-protein electron transfer, Protein-protein docking, FNR/Fd, FNR/Fld, QM/MM e-

pathway, electronic coupling

1. INTRODUCTION

Electron transfer (ET) reactions are key processes in all type of biological systems, being the mitochondrial and photosynthetic protein-protein ET chains of particular relevance in the bioenergetics metabolism of cells [1-3]; thus, understanding their mechanisms and biological function is crucial in medical and bioengineering applications. In spite of its key role in living organisms, ET between redox protein partners is largely unknown at the molecular level [4-7]. Majority of ET mechanistic studies rely on the availability of 3D-crystallographic structures, most feasible for intra-protein process. However, modelling ET between two (or more) proteins becomes more complex. Besides, from defining the ET pathway and estimating the rate, the challenge arises from the dynamic nature of the (typically) weak binding process, leading to formation of "optimal protein-protein complex" subsequently followed by rapid transferring of the electron(s) [8].

We are particularly interested in the photosynthetic ET chain and, more in detail, in the two electrons transfer from photosystem I (PSI) to the flavin-dependent ferredoxin-NADP$^+$ reductase (FNR, ~303 residues) via the action of two sequential independent ferredoxin (Fd) electron carriers [9, 10]. In general, the catalytic process in FNR involves the reduction of its flavin adenine dinucleotide (FAD quinone form), a prosthetic group non-covalently bound to FNR, to the one-electron reduced radical (FADH$^•$ semiquinone form), followed by its further reduction to fully reduced FAD hydroquinone (FADH$^-$ hydroquinone form) [9-11]. These reductions are performed sequentially by two Fd molecules, delivering each one electron to FNR at a single binding site. Fd is a small electron carrier protein (~98 residues) that contains an iron-sulphur cluster (FES) as redox center [12, 13].

In some algae and cyanobacteria (as *Anabaena*), under low iron conditions, flavodoxin (Fld) replaces Fd as single electron carrier [10, 14]. Fld is a medium-small electron carrier protein with 169 residues containing a flavin mononucleotide (FMN) as a redox cofactor. Although, Fd and Fld are different in molecular size, sequence and redox cofactors, FES in Fd and FMN in Fld, they are able to play similar roles in this ET chain, interacting with FNR at the same binding site and with slightly lower efficiency when using Fld ($K_d^{PPartner}$ and k_{ET} values for the reduction of FNR are ~1.3 μM and ~6200 s^{-1}, respectively, when using Fd as electron donor and ~3 μM and >600 s^{-1}, respectively, when using Fld) [9, 15-20].

Site-directed mutations in *Anabaena* FNR revealed that positively charged residues at positions R16, K72 and, particularly, K75 as well as hydrophobic residues at L76, L78

and V136, are critical for efficient interaction, and therefore contribute to an efficient ET, with both Fd and Fld (Fig. 1), while other residues also situated on the protein surface, K138E, R264E, K290E, and K294E, contribute to the interaction in lesser extent [9, 15, 16, 21-24]. Similarly for Fd, a negatively charged side chain at position E94, a hydrophobic side chain at position F65 and S47 are crucial for the electron transfer process by controlling the specific orientations of Fd and FNR within the transient electron-transfer complex [25-29].

In contrast, mutagenesis studies on Fld have shown that even though several residues modulate Fld interaction with FNR, none appear critical neither to produce the competent protein-protein complex nor for ET process itself [15, 19, 24, 30]. Despite of extensive mutational studies to characterize FNR/Fd and FNR/Fld complexes [16, 21, 22, 31, 32], only FNR/Fd X-ray structures from *Anabaena* and maize have been solved [33, 34]; structural data for FNR/Fld remains elusive. An FNR/Fld bound model, however, has been proposed based on the high homology between two different domains of cytochrome P450 reductase (CPR) with FNR and Fld [35].

Computer simulations are entering nowadays in most biophysical and biochemical studies. Our laboratory has recently shown how theoretical simulations are mature enough to provide quantitative descriptions of complex ET processes. Using a multiscale approach combining classical and quantum simulations, together with analytical electron coupling calculations, we can provide accurate mechanism and rate information for protein-protein ET [7]. These techniques, however, demanded the presence of an X-ray structure. In this paper we add an additional layer, based on a coarse-grained potential Monte Carlo docking, capable of describing the formation of protein complexes. The overall approach uses a 'funnel filtering' scheme (Scheme 1). Our analysis reveals the underlying mechanism of ET in FNR/Fd proceeding through a 'protein mediated mechanism' where tunneling of the electron from Fd to FNR is facilitated by loop-residues 40-49 of Fd. In FNR/Fld, however, ET is a direct transfer between redox cofactors and less complex specific than in Fd; more than one orientation in the encounter complex can be efficient in ET.
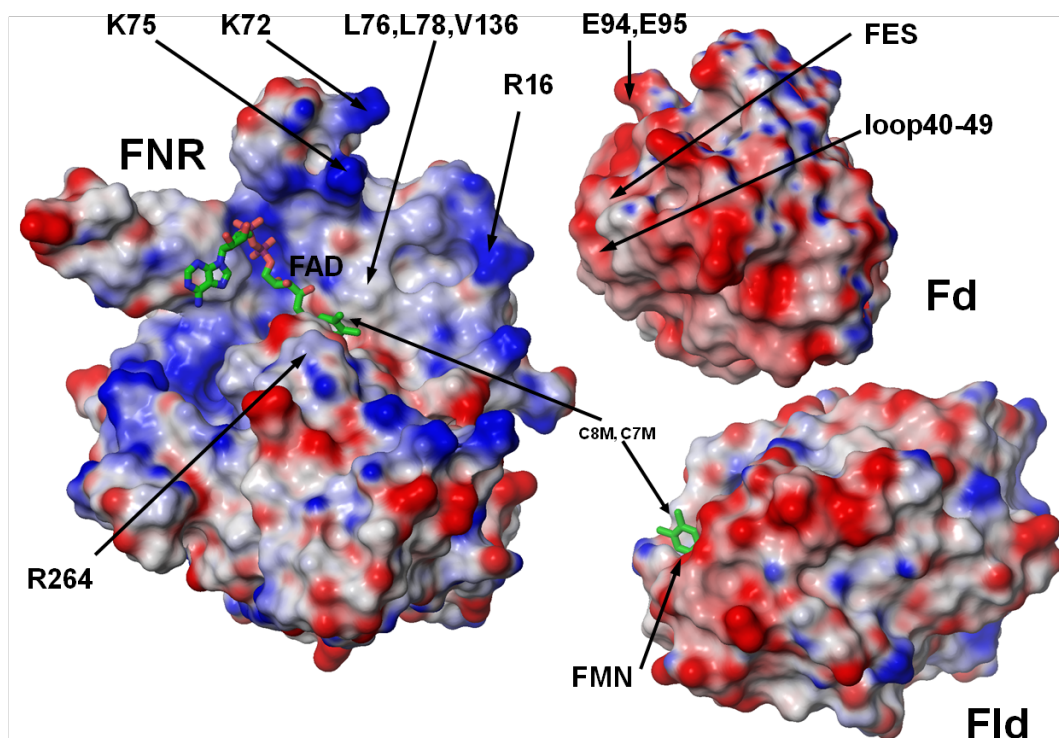
Figure 1. The electrostatic potential surface of *Anabaena* FNR, Fd and Fld computed from APBS program. The cofactors; FAD, FES and FMN are drawn in stick representation. Critical positions for positively charged residues on FNR and negative ones on Fd are depicted. Fd and Fld are highly negatively charged proteins consisting of 22% (22 out of 98 residues) and 18% (31 out of 169 residues) aspartic and glutamic residues on the protein surface, respectively.

2. METHOD

We have developed a protocol for effectively exploring the conformational ensemble of protein-protein ET complex by applying a 'funnel filtering' scheme composed of (i) coarse-grained (CG) protein-protein docking, (ii) all-atom classical force field refinement, (iii) electron transfer pathways through the quantum mechanic/molecular mechanic (QM/MM) e-Pathway approach, and iv) QM/MM electronic coupling (Hda) calculations to determine the ET efficiency (Scheme 1). Initially, the X-ray crystal structure of the FNR/Fd complex was used as a reference to validate and adjust the performance of our developed protein-protein docking protocol, then the same protocol was applied to model the FNR/Fld interaction.
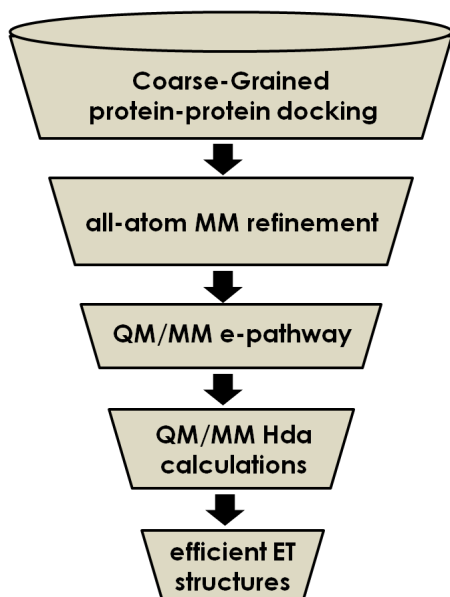
Scheme 1. The '*funnel filtering*' scheme to efficiently map the protein-protein ET mechanism.

Initial Model

The reference structure for the FNR/Fd system was obtained from the X-ray structure of the *Anabaena* FNR/Fd complex (PDB code 1EWY) [36]. The reference structure for the FNR/Fld system was built by superimposition of *Anabaena* FNR (extracted FNR from 1EWY) and Fld (1FLV) [37, 38] on to the crystal structure of cytochrome P450 reductase (CPR) [39], a multi-domain protein with two domains highly homologous to FNR and Fld. Protein preparation was done using the Protein Wizard [40] within the Schrödinger Suite to optimize hydrogen bond networks and assign proper protonation states for ionizable residues at pH 7.0.

2.1 Coarse-Grained protein-protein docking

We have developed a protein-protein docking procedure consisting of a rigid body Monte Carlo search sampling with a CG model. Complete details for the methodology are given in supporting Information. In brief, our CG model is based on the parameterization introduced by Basdevant *et. al*. [41] where each amino acid is described using one to three beads with an additive potential energy function including distinct van der Waals (vdW) and Coulombic terms. This procedure has been successfully applied to model the tryptogalinin-trypsin complex interactions [42]. In this paper, we enhance sampling by adding a restraint between the two redox centers, limiting in this way the maximum distance for ET. Such addition allowed a more effective sampling of the complex space. In

addition, a discrete protonation criterion was also implemented in the CG sampling to take into account possible pKa changes of surface negative residues upon complex formation. In particular, for each conformation (and before scoring takes place), if two negatively charged surface residues from protein A (FNR) and B (Fd or Fld) are within 6 Å, measured as side chain bead distance, the ligand residue gets protonated to its neutral state (in a similar approach to the one used by PROPKA [43]. This procedure reduced repulsive interactions between negatively charged beads along the protein-protein interface eliminating false negatives.

2.2 All-atom MM refinement

Total of 1500 lowest energetic structures from the CG protein-protein sampling were filtered for further all-atom refinement to remove possible atomic clashes and re-optimize the hydrogen bond networks. This step was composed of performing: (i) protein preparation using the Protein Wizard [40], and (ii) all-atom minimization using PELE (Protein Energy Landscape Exploration) [44, 45]. This procedure has been used previously to improve scoring functions in protein-protein docking [46]. In particular, and because of the highly negatively charged surfaces in Fd and Fld (Fig. 1), the pKa of titratable residues was analyzed at an all-atom level using PROPKA and different protonation states adapted accordingly. Minimization parameters included using the 2005 OPLS-AA force field with the OBC implicit solvent [47], 0.15 mol/L ionic strength and fixing all alpha carbons. The lowest energy complex at each RMSD value (one unit binning) ranging from 1 to 20 Å RMSD to the reference complexes were selected for the last step of the QM/MM e-Pathway and electronic coupling calculations to elucidate the reactive ET conformations. Detailed methodology is described in Supporting Information.

2.3 The ET mechanism: QM/MM e-Pathway and Electronic coupling (Hda) calculations

All QM/MM calculations were carried out using QSite from the Schrödinger suite (QSite, version 5.7; Schrödinger, LLC:New York). Structures selected after all-atom MM refinement including X-ray and reference structures were studied. The geometries of FNR/Fd and FNR/Fld systems were optimized using the spin unrestricted DFT method with the M06 functional [48] and the lacvp(d,p) basis set. Atoms in the MM region were treated with the OPLS (optimized potential for liquid simulations) force field. The hydrogen link atom approach was used for the QM/MM boundary treatment. During the QM/MM geometry optimization, the QM region and all-atoms within the distance of 10 Å from any

atom in redox cofactors (FAD, FES and FMN) were allowed to relax.

The QM/MM e-Pathway

ET pathways were identified using the QM/MM e-Pathway approach [7, 49, 50], where the ET region between the donor and acceptor is described by QM while the rest is treated at the MM level of theory. Briefly, the method strategy is based on iteratively modifying the QM region (moving residues from the QM region to the MM one), and following the evolution of the spin density of an unpaired electron. The method assumes that this unpaired electron has left the donor site but has not yet arrived to the acceptor site. Thus, the donor and acceptor sites, included in the MM region, are defined in the oxidized form. The iterative search stops once the donor and the acceptor can be connected through a direct pathway built upon joining the identified molecular orbital. These orbitals, identifying residues that may play a major role in the ET process, form the main output of this technique.

The QM/MM electronic coupling (Hda) calculations

Electronic coupling (Hda) values were calculated using the Fragment Charge Difference (FCD) method [7, 51] through the e-coupling server (http://ecouplingserver.bsc.es). Larger values of Hda reflect stronger coupling between donor and acceptor molecular orbitals, hence suggesting higher ET efficiency. Here, all residues identified from the QM/MM e-Pathway and the donor and acceptor sites were included into the QM region, resulting in a total of 176 and 69 atoms for the FNR/Fd and FR/Fld systems, respectively. To account for nearly-degenerated states, we computed the root mean square coupling (*rmsd*Hda) according to Voityuk et al. [52].

Molecular dynamics simulations

MD simulations were performed with Desmond [53]. The structures were solvated in an orthorhombic box, with a buffer solvent region of at least 10 Å. The system was then neutralized, and an ionic force of 0.15 M was set by adding 65 Na^+ and 45 Cl^- ions. The default relaxation protocol in Desmond was used followed by production runs using NPT ensemble with a Martyna-Tobias-Klein barostat and a Nose-Hoover thermostat. The temperature was set to 300 K with a 2 fs time-step, SHAKE on hydrogen atoms and long-range Ewald summation. Atomic charges for the cofactor molecules were obtained from the QM/MM electrostatic potential fitting.

3. RESULTS

3.1 Protein-protein docking

3.1.1 FNR/Fd complex

In our initial attempt to apply our CG sampling for the FNR/Fd complex, where a reference crystal structure exists, we obtained good cofactor distances, in the range of 9.5-12.4 Å. Moreover, the reference X-ray structure was always lower in energy, -i.e. no false positives were produced. However, the CG sampling was not able to positively score near native structures with RMSD less than 4 Å (Fig. 2A). Structural analysis of the low RMSD rejected structures showed negatively charged residues (GLU and ASP) at the binding interface in close proximity. These introduced a large repulsive interaction since our CG initial model kept them always deprotonated. PROPKA predictions, however clearly determine one of them to be protonated, because of the electrostatic interaction between pair-wise negatively charged residues. Modification of our sampling algorithms to take such effect into account (see Methods) resulted in a significant improvement of the CG sampling with acceptance of low energetic conformations with RMSD less than 4 Å (Fig. 2B). The near native conformation with a RMSD of 1.4 Å from the X-ray reference is now ranked as the best solution. Moreover, among the top 10-lowest energy solutions, we find four additional structures resembling the X-ray complex (with RMSD < 3 Å), together with two other distinct minima at 13 and 19 Å RMSD. Importantly, in the subsequent all-atom refinement, the funnel correlation between the binding energy and the RMSD against the native X-ray structure is better observed (Fig. 2C). Notice as well that the X-ray structure was also minimized, with a consequent small RMSD displacement of 1.0 Å. This result indicates good correlation between CG and all-atom energy functions and validates the faster CG screening of the number of candidates to be scored by all-atom techniques.

The lowest RMSD poses (< 4 Å) share the same interaction site as the X-ray one, forming strong hydrogen bonds between Fd:E94/E95 with FNR:K72 or FNR:K75, and Fd:D67/D69 with FNR:R16, as well as hydrophobic interactions between F65 on Fd with L76, L78 and V136 on FNR (Fig. S1 and Table S1). These residues on FNR and Fd have been identified to be critical for protein-protein interactions by mutational studies [10, 15, 16]. Other conformational minima orient different negatively charged residues on Fd surface to interact with K72, K75 and R16 on FNR, such as Fd:D31/D36 or Fd:D62/D67/D69 (Table S1). Mutations at these Fd residues also produce moderate effect on complex stability and ET with the reductase [23]. To gain insight on the ET efficiency across the whole range of RMSD structures, the lowest energy conformation for each 1 Å RMSD-window (1 - 20 Å) were selected for further QM/MM ET calculations (results shown

below). Notice that the 0-1 Å RMSD window structure corresponds to the minimized X-ray one, not being a real prediction and only used for comparison. These candidate structures show multiple orientations of Fd binding on FNR, but all share Fd´s loop residues 40-49 at the interface with FNR and thus have the redox distance between FAD and FES around 7 - 10 Å (measured between FAD:C8M•••FES:Fe1 atoms) (Fig. 2D and Table S1).
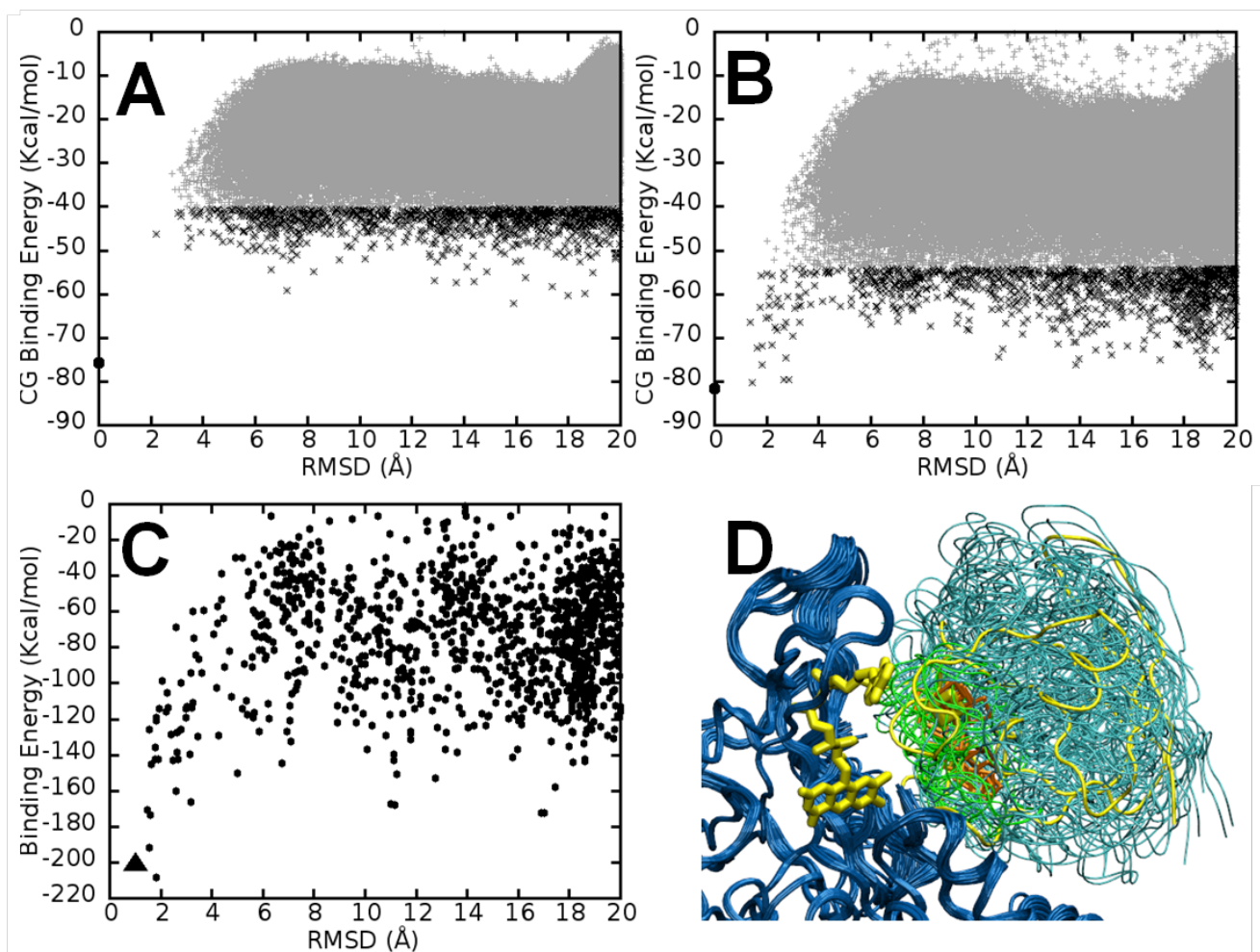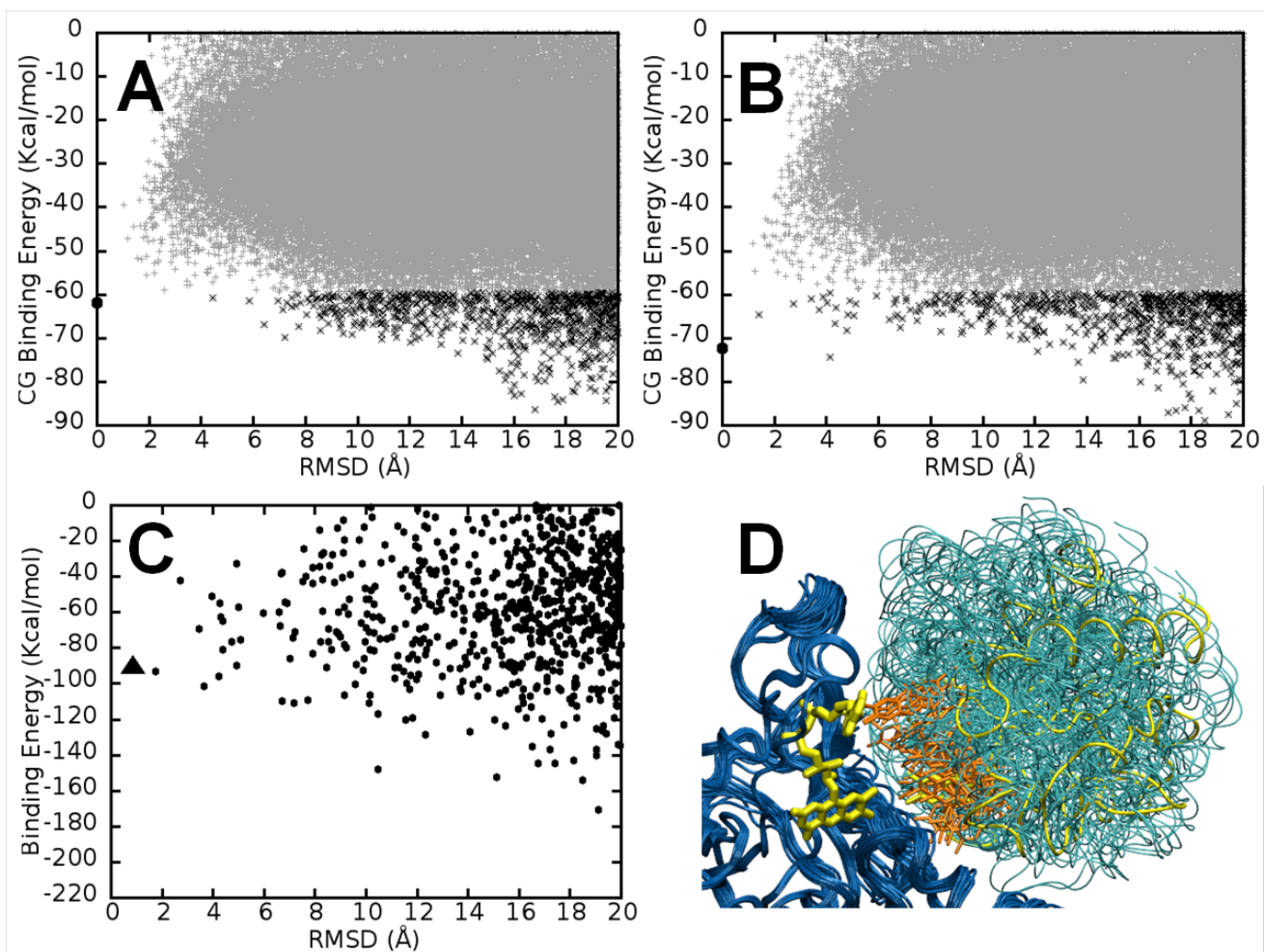

Figure 2. FNR/Fd complex sampling. Plots of CG docking binding energy versus RMSD to the reference X-Ray structure without (A) and with (B) re-protonation of surface charged residues. The reference is marked with big black dot at 0 Å RMSD. The top 1500 structures selected for the following all-atom refinements are underlined darker. (C) The plot of the top 1500 refined all-atom binding energy versus the same RMSD. The minimized reference (notice the slight displacement from the 0 Å RMSD value) is marked with black triangle. (D) Superimposition of 20 lowest energy structures representing each 1 Å RMSD window from the all-atom refinement. The reference structure is shown in yellow color. FNR protein is in dark blue, Fd protein is in cyan, FES of Fd is in orange, the loop-residue 40-49 of Fd is in green.

3.1.2 FNR/Fld complex

The CG sampling protocol fitted with the FNR/Fd complex was applied to model the interactions of the FNR/Fld complex, for which crystallographic structure is unknown. Contrary to the Fd complex, now we do not obtain a funnel-shaped correlation between binding energy and RMSD toward the reference homology model (Fig. 3A and 3B). For Fld, we observe a weaker contribution from negatively charged residues, with smaller effects on the FNR/Fld CG sampling. The complexes obtained present conformations with FAD-FMN cofactor distances within a range of 4 – 10 Å (measured between the geometrical centers of FAD:C8M/C7M atoms and FMN:C8M/C7M atoms). The 10 lowest energy conformations are drastically different from the reference model, with 18 - 20 Å RMSD values, and present cofactor distances in the 5.5 - 8.5 Å range, not as short as in the reference model (4.3 Å). Upon all-atom refinement, the overall picture of predicted complexes does not change; the best pose is 19 Å RMSD from the homology reference structure (Fig. 3C). Interestingly, the best energy complexes show more interface contacts involving experimentally identified critical charged residues on FNR: K72, K75 and R16 as well as key hydrophobic residues (L76, L78 and V136), see Table S2. Superposition of the lowest energy conformation at each 1 Å RMSD intervals in the all-atom refinement is shown in Fig. 3D. They present multiple binding orientations of Fld, having the FMN cofactor in a direct contact with FNR protein.

While the reference model has the shortest distance (by 1.5 Å) between FAD and FMN, it represents a significant higher energy pose. Interestingly, there are several alternative orientations, for instance structures at RMSD of 9, 12, and 19 Å, which bring the FAD and FMN rings into close distances and are associated to lower complex energies (Table S2), which may dominate ET. As in Fd, we selected the 20 lowest energy conformations for each 1 Å RMSD-window (1-20 Å, with the 0-1 structure corresponding to the minimized CPR-homology reference) for further QM/MM e-Pathway and electronic coupling calculations.

Figure 3. FNR/Fld complex sampling. Plots of CG docking binding energy versus RMSD to the reference homology structure without (A) and with (B) re-protonation of surface charged residues. The reference is marked with big black dot at 0 Å RMSD. The top 1500 structures selected for the following all-atom refinements are underlined darker. (C) The plot of all-atom refinement binding energy versus RMSD. The minimized reference (notice the slight displacement from the 0 Å RMSD value) is marked with black triangle. (D) Superimposition of 20 lowest energy structures representing each 1 Å RMSD window from the all-atom refinement. The reference structure is shown in yellow. FNR protein is in dark blue, Fld protein is in cyan, FMN of Fld is in orange.

3.2 ET mechanism

3.2.1 ET pathway in FNR/Fd complex

Fig. 4 shows the electron transfer pathway obtained by the QM/MM e-pathway method in the FNR/Fd X-ray complex. Our results indicate a pathway involving L78 on FNR, F65 and the loop-residues 40-49 on Fd, located at the interface between the two proteins. In order to quantify the impact of single residues on the ET pathway, we calculated the electronic coupling (Hda) values by including/excluding those residues from

11

the quantum region in bridge-mediated electronic coupling QM/MM calculations. The results of Hda on different QM models, varying from a smallest model by including only the donor and acceptor sites to larger expanded models including more specified bridging residues, are shown in Table 1. They clearly reveal that when adding loop-residues 40-49 of Fd into the quantum region, M3 to M5 rows in Table 1, the electronic coupling is significantly increased ~30 fold, compared to the direct donor-acceptor coupling (M1 and M2 rows). Such Hda rise translates to a ~3-order of magnitude increase in the rate constant for ET (k_{ET}), estimated via the Marcus theory assuming same values for reaction free energy and reorganization energy. Thus, our result suggests that the ET mechanism in FNR/Fd is based on a "*bridge-mediated ET*" including loop 40-49 of Fd. We note that, adding F65 of Fd, L78 of FNR and more adjacent residues does not significantly improve Hda values.
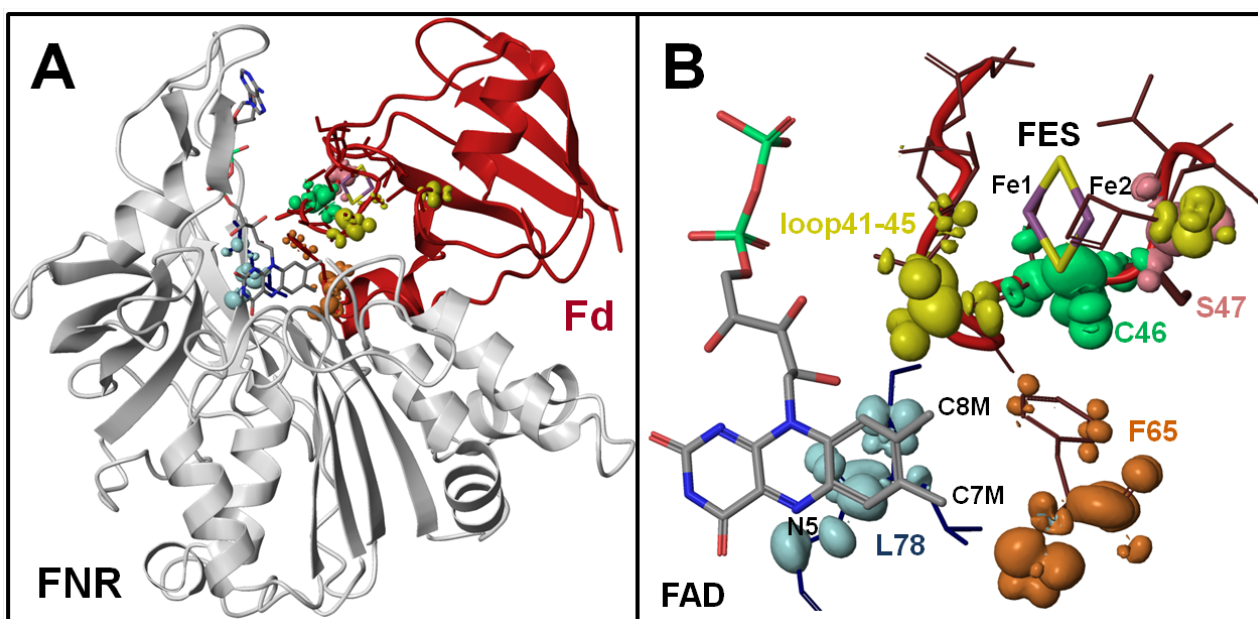
Figure 4. Electron transfer pathway in FNR/Fd X-ray complex. One electron is transferred from the FES cluster (Fd) to the FAD flavin ring (FNR) through the loop involving residues 40-49 on Fd based on the X-ray. Each different color corresponds to the spin density identified in a separate QM/MM e-pathway iteration. Residues are identified in the following order: F65 of Fd (orange), L78 of FNR (light blue), backbone atoms of C46 (green) and S47 of Fd (pink), backbone atoms of the loop-residue 41-45 of Fd (yellow). The residues of Fd are colored in red and L78 of FNR in blue, respectively.

Table 1. Electronic coupling (Hda) calculated on the FNR/Fd X-ray complex based on the derived QM/MM e-pathway.

model	residues included in QM	Hda (eV)
M1[a]	mFAD+ FES + C41 + C46 + C49 + C79	7.31×10^{-5}
M2[b]	M1 + C41 + C46 + C49 + C79	8.68×10^{-5}
M3	M2 + loop-residue C40-C49	2.36×10^{-3}
M4	M3 + F65	2.40×10^{-3}
M5	M4 + L78	2.31×10^{-3}

[a]only the side chains of cysteine residues are included in QM part.

[b]entire cysteine residues are included in QM part.

We further examine the ET pathway and efficiency (Hda calculations) on the different conformations selected after the all-atom refinement. These structures have Fd bound to FNR in diverse orientations, but they share a common feature where the loop-residues 40-49 on Fd lies between the FAD and the FES redox centers, with distances between them around 7-10 Å (details given in Table S1). For all structures, the QM/MM e-pathway method allocates spin density on several residues of the Fd loop, suggesting their role in the ET pathway.

By defining the same QM region (M4) as in the X-ray structure, Hda values calculated over 20 structures are ranged from 10^{-5} to 10^{-3} eV. Overall, Hda values correlate well with the conformational RMSD (Fig. 5A) and even better with the distance between redox centers (Fig. 5B). The X-ray configuration (R00 structure, window 0-1 Å) provides the highest Hda value with 2.97×10^{-3} eV. Nevertheless 4 predicted structures, with mid-low RMSD and redox distance values provide similar electronic coupling to the reference structure. Among the similar structures to the X-ray (1-4 Å RMSD), for example, the R03 structure, with 3.2 Å RMSD and 8.9 Å distance, produces the highest fully predicted Hda value: 2.22×10^{-3} eV (Fig. 5A). Although R01 and R02 closely resemble the X-ray orientation, RMSD < 2 Å, their redox distances are further away, 8.0 Å in the X-ray and 9.5 Å in both R02 and R03 structures, resulting in low Hda values: 4.17×10^{-4} eV and 6.73×10^{-5} eV, respectively. This result suggests that even within similar conformations, ET efficiency is very sensitive to the distance parameter between redox centers. Besides the X-ray and R03 structures, conformations with RMSD of 7, 8 and 10 Å (R07, R08 and R10, respectively) have similar values to the reference one (~10^{-3} eV). Although such structures

present Fd bound to FNR in different orientations, they all bring FAD and FES redox centers into close distance, 7.0-7.7 Å. Analysis of the interface region for all high Hda structures (R00, R03, R07, R08 and R10) indicate a major role of experimentally determined critical residues [10, 15, 16]. For instance, the X-ray, R03 and R07 have FNR:K75 interacting with Fd:E94, FNR:R16 interacting with Fd:D67/D69, and hydrophobic contact between FNR:L76/L78/V136 with Fd:F65 are conserved (Table S1 and Fig. S1). Although R08 and R10 have Fd binding with different orientation, almost a 180 degree turn, critical residues contacts still remains: FNR:R16 interacts with Fd:E94/E95 and FNR:K72/K75 interacts with Fd:D36. The hydrophobic region on FNR interacts with backbone of the loop-residue 40-45.
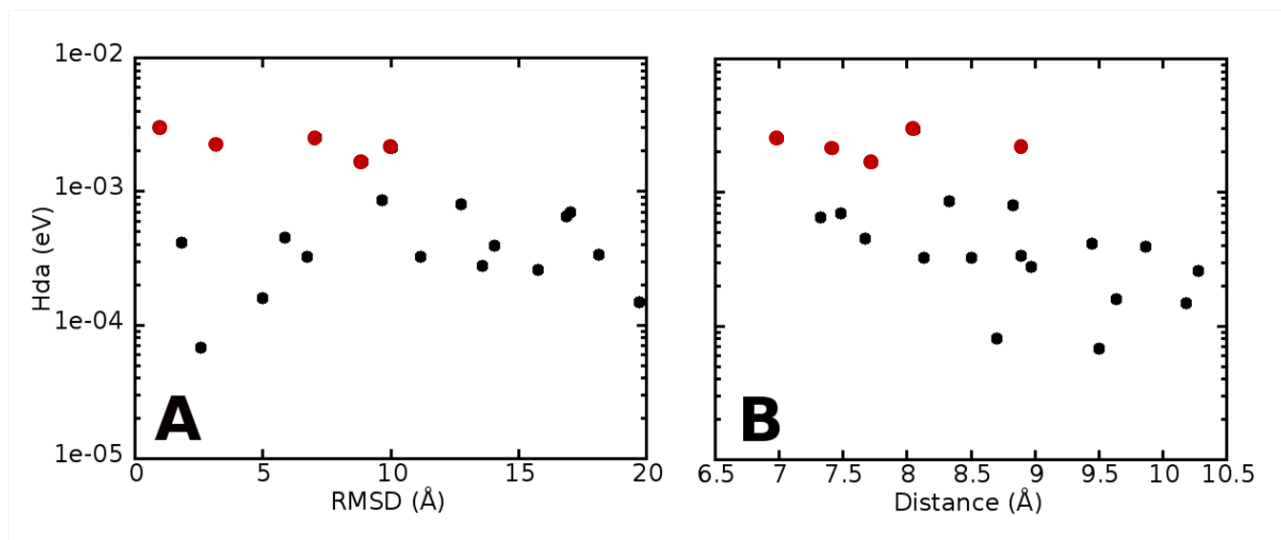
Figure 5. Logarithm plot of the Hda obtained from the 20 FNR/Fd structures selected in the all-atom refinement versus the RMSD to the reference crystal (A) and the redox distance (B). Redox distance is measured between FAD:C8M•••FES:Fe1. Relatively high Hda values are colored in red.

**The mutational effect at F65 and S47 of Fd**

Experimental data indicate that replacement of F65 by A or I completely prevents ET, while F or Y mutants remain active as the WT. Similarly, replacement of S47 by A or T produces inactive proteins for ET [23]. We modeled these mutational effects by performing 1-ns MD simulations on the R00 (X-ray configuration of FNR/Fd complex) for the Fd WT, F65A, F65Y, S47A and S47T complexes. Table 2 shows the average Hda values along the MD simulations using the M5 model (~200 atoms in the QM region). Consistent with experimental results, an aromatic amino acid at position 65 does not affect Hda. On the other site, the F65A mutant reduces Hda by 50%, translating into a reduction

of k_{ET} by ~1-order of magnitude. In S47A and S47T mutants, the average Hda values are 4.7 and 6.2-fold reduced compared to the WT, which approximately implied to reduced k_{ET} by 2-order of magnitude. In the WT, the hydroxyl side chain of S47 is hydrogen-bonded to E94 and Y98 in Fd anchoring the FES binding loop to the protein. The two mutations at position S47 disturb this hydrogen-bonded network and the conformation of loop-residues 40-49 on Fd.

Structural analysis of the MD trajectories reveals a significant distortion of the protein-protein binding interface for the F65A, S47A and S47T Fd mutants. We should keep in mind that we only performed 1 ns simulation, and we can only analyze tendencies; longer simulations might introduce a larger disruption on the protein-protein interface which, as shown above, leads to big effects on the electronic coupling and on the ET rate. Nevertheless, as seen in Fig. 6 for the F65A mutant, the short simulation clearly affects the binding interface, with a significant entrance of water molecules. Such weakening of the protein-protein complex formation correlates well with the 10-fold larger dissociation constant (120 vs. 9.4 μM) seen for the F65A mutant [28].

Table 2: Hda from a 1-ns MD for the Fd WT and F65A, F65Y, S47A and S47T mutants.

| Hda (eV)	WT (F65)	F65A	F65Y	S47A	S47T
averaged MD	1.269×10^{-3}	5.314×10^{-4}	1.475×10^{-3}	2.721×10^{-4}	2.033×10^{-4}
std.	0.213×10^{-3}	0.252×10^{-4}	0.081×10^{-3}	2.123×10^{-4}	2.438×10^{-4}
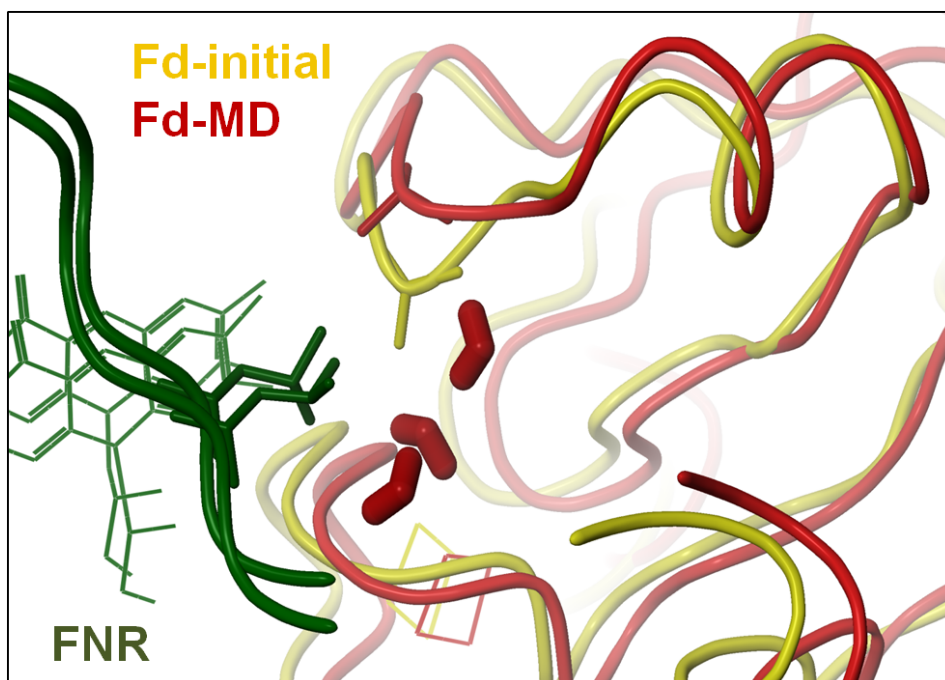
Figure 6. Initial (yellow) and final (red, after MD) Fd structures for the F65A mutant.

Entrance of three water molecules into the protein-protein interface is also shown. Fd:A65 and FNR:L78 are shown in sticks.

3.2.2 ET pathway in FNR/Fld complex

In FNR and Fld (contrary to Fd), we find FAD and FMN cofactors with partial solvent exposure, in particular at the two methyl groups of the isoalloxazine ring (C7M and C8M), as shown in Fig. 1. In several docking conformations, including the reference CPR-based homology model, we find that the methyl groups of FMN and FAD are within direct van de Waals contact (atomic distances are given in Table S2). In Fig. 7, the QM/MM optimization of the reference structure clearly illustrates the overlapping of the HOMO molecular orbital in FAD and FMN cofactors suggesting that ET in the FNR/Fld complex can easily proceed through a '*direct ET*' mechanism where electron directly jumps from FMN to FAD without involving any protein molecular orbital acting in a bridge-mediated ET mechanism.
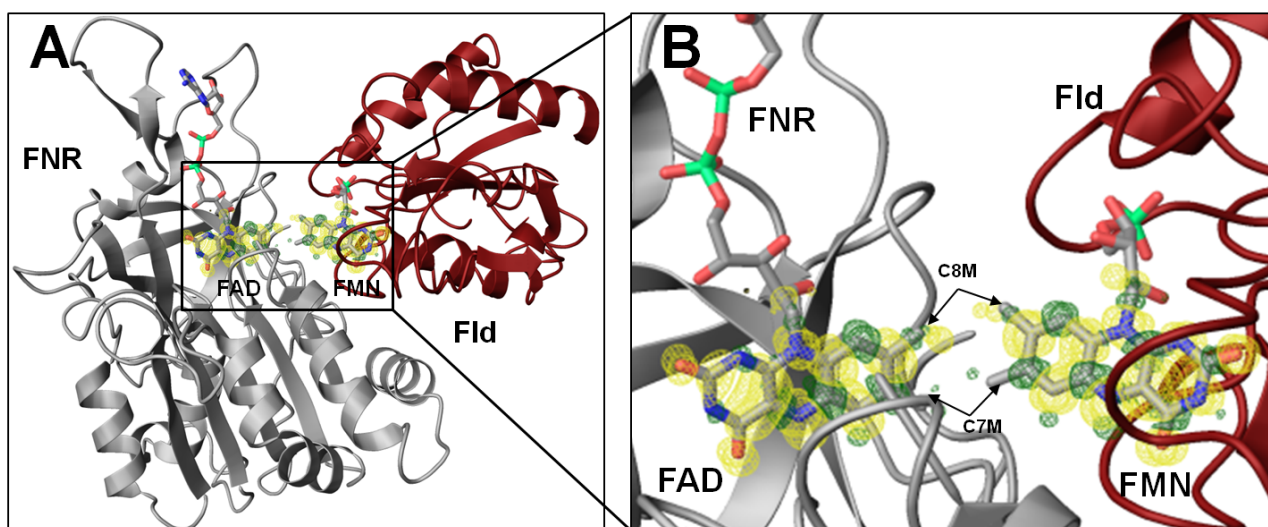

Figure 7. Visualization of HOMO molecular orbital overlap between the FAD and FMN cofactors, (A) reference CPR-based homology FNR/Fld model and (B) zoom-in cofactors site.

Due to the previous analysis, Hda calculations initially included only the flavin rings of FAD and FMN to the QM region. Electron coupling values show strong correlation with the redox cofactors distance, while we see none with Fld orientation (RMSD) with respect to the reference CPR-based homology model (Fig 8). While structures close to the reference model (RMSD < 4 Å), provide large electronic coupling, structures R09, R12 and R19, with RMSD of 9, 12 and 19 Å, respectively, also produce large Hda values (>10^{-3} eV). Although, these structures reveal distinct Fld orientations, they all share a close

contact between FAD and FMN < 7 Å (Fig. 8B).

Some docking poses with larger cofactor distances (> 9 Å) have a protein side chain mediating contact between them (i.e. Y94 or W57 on Fld). Those structures resulted in small Hda (< 10^{-5} eV) when considering a direct ET process between FMN and FAD. Including these bridge residues in the QM calculation improves Hda by 1-order of magnitude (opened-circles on Fig. 8), but does not introduce new high values. This is in agreement with mutational studies indicating that Y94 and W57 do not play a role in the protein-protein ET process even if they affect the Fld redox potential [15].
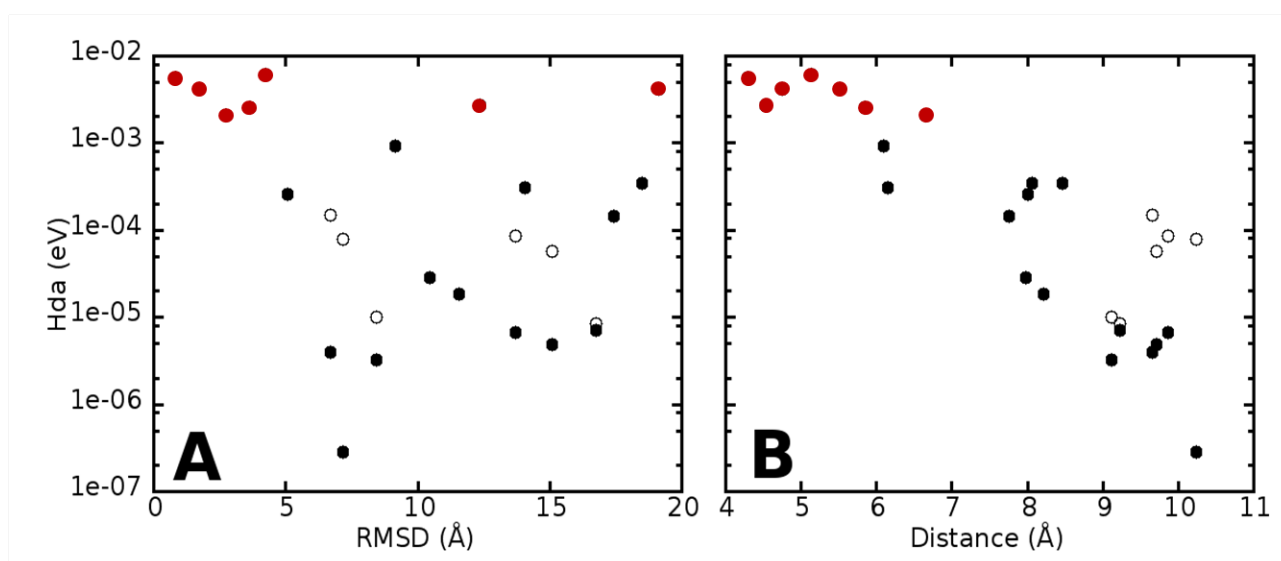
Figure 8. Logarithm plot of Hda obtained from the 20 FNR/Fld structures selected in the all-atom refinement versus the alpha carbon RMSD to the reference crystal (A) and the redox distance (B). Redox distance is measured between the geometrical centers of FAD:C8M/C7M atoms and FMN:C8M/C7M atoms. Relatively high Hda values are colored in red and opened-circles indicate Hda when including Y94 or W57 in the QM region (see main text).

4. DISCUSSION

Extensive mutational studies have characterized the protein-protein interaction and ET mechanism in FNR/Fd and FNR/Fld complexes. Interestingly, even though Fd and Fld share the interaction site on FNR, individual residues on FNR do not participate to the same extent in the interaction with each of the protein partners, pointing to different electron transfer mechanisms [10, 15, 16, 23, 24]. The lack of critical residues (for both complex formation and ET) on Fld has suggested a less specific interaction than that of Fd. Since we only have an X-ray crystal structure for FNR/Fd complex [33, 34], it is difficult to establish a molecular basis leading to the possible different ET mechanism. Such

comprehensive analysis, however, can be provided by recent developments in multiscale computational modeling [7, 41, 51].

Comparing protein-protein interaction energies, both at the CG (Fig. 2B–Fig. 3B) and all-atom level (Fig. 2C–Fig. 3C), we see how the interaction in Fld is less specific than that in Fd. Fd presents a deeper minimum that should dominate the protein-protein interaction. In addition, best interaction energies are predicted in the vicinity of the reference crystal; we remind here that no information on the crystal FNR/Fd structure (other than for comparison purpose) is used along the protein-protein sampling. Fld, on the contrary, has a larger range of orientations showing similar interaction energies. Such initial biophysical analysis seems to agree with the less specific FNR/Fld interaction scenario proposed from mutational analyses. For it to work, it will require large electronic coupling values for the FNR/Fd X-ray complex and for several of the less specific FNR/Fld complexes. To address this issue, we turn into mixed QM/MM simulations.

In FNR/Fd, the QM/MM e-pathway results indicate a bridge-mediated ET mechanism through the Fd loop involving residues 40-49. Moreover, electronic coupling calculations confirm the active role of this loop in assisting the ET process. Importantly, Hda values are correlated with the RMSD to the X-ray complex (as well as to the redox centers distance, an expected result in ET). In addition, structures with high Hda values show interaction between residues experimentally detected as critical. In this sense, conformations with distinct Fd orientations but short redox distances, for instance R05, R16 and R17, do not preserve these interactions and produce low Hda values. Thus, from an electronic coupling point of view, FNR/Fd efficient ET configurations are limited to a small fraction placing the Fd loop at the interface and short donor acceptor distances. Among them we find various structures: R00, R03, R07, R08 and R10 ($\sim 10^{-3}$ eV), but the near-native conformations (R00 and R03) present significant lower protein-protein binding energies. Thus, when adding the protein-protein interaction biophysical analysis, it clearly discriminates an ensemble of structures similar to the X-ray one.

In the FNR/Fld complex we have a rather different scenario. The strong correlation between Hda values and the cofactor distance, together with the HOMO molecular orbital overlap seen in Fig. 7, strongly suggest a direct ET mechanism between FAD and FMN. Only conformations having significantly short distance (within a van de Waals contact between cofactors) result in large Hda values. Amongst these large electronic couplings complexes, however, we find structures with different Fld orientations. In addition, we see slightly larger Hda values in FNR/Fld than in FNR/Fd, in agreement with the less pronounced minima observed in the protein-protein interaction analysis (requiring a faster

ET process), and with the (also slightly) weaker experimental binding energies (K_A of 7.6 × 10^5 and 3.5 × 10^5 M^{-1} for FNR/Fd and FNR/Fld, respectively[54]). In these regards, while the CPR-homology reference has weaker protein-protein interaction energies, it presents high Hda values. Thus, our simulations support the *transient bound conformation* mechanism proposed previously for the FNR/Fld ET process [8, 15, 19, 24, 30, 55, 56]. In this model, Fld binds on FNR in a variety of docked conformations, with ET involving a subset of (diverse) highly reactive conformations where the redox cofactors are in direct contact.

In conclusion, our results obtained from multiscale modelling including coarse-grained and all-atom protein-protein docking, QM/MM e-pathway and electronic coupling calculations, allow for a molecular and electronic comprehensive analysis of the ET process in FNR/Fd and FNR/Fld complexes. Our results, consistent with experimental mutational data, assign a bridge-mediated ET mechanism with a more stable and dominant complex for FNR/Fd, and a direct ET mechanism with transient and less-specific complexes in FNR/Fld.

5. References

1. Gray, H.B. and J.R. Winkler, *Electron flow through metalloproteins.* Biochimica et Biophysica Acta (BBA) - Bioenergetics, 2010. **1797**(9): p. 1563–1572.
2. Moser, C.C., J.L.R. Anderson, and P.L. Dutton, *Guidelines for tunneling in enzymes.* Biochimica et Biophysica Acta (BBA) - Bioenergetics, 2010. **1797**(9): p. 1573–1586.
3. Page, C.C., C.C. Moser, and P.L. Dutton, *Mechanism for electron transfer within and between proteins.* Current Opinion in Chemical Biology, 2003. **7**(5): p. 551–556.
4. Beratan, D.N., et al., *Electron-tunneling pathways in proteins.* Science, 1992. **258**(5089): p. 1740-1741.
5. Hayashi, T. and A.A. Stuchebrukhov, *Electron tunneling in respiratory complex I.* Proc. Natl. Acad. Sci. U. S. A., 2010. **107**(45): p. 19157-19162.
6. Kitoh-Nishioka, H. and K. Ando, *Fragment Molecular Orbital Study on Electron Tunneling Mechanisms in Bacterial Photosynthetic Reaction Center.* J. Phys. Chem. B, 2012. **116**(43): p. 12933–12945.
7. Wallrapp, F., A. Voytiuk, and V. Guallar, *In-silico Assessment of protein-protein electron transfer. A case study: Cytochrome c Peroxidase - cytochrome c.* Plos Comput. Biol., 2013. **9**: p. e1002990.
8. Ubbink, M., *Dynamics in transient complexes of redox proteins.* Biochem. Soc. Trans.,

2012. **40**(2): p. 415-8.

9. Carrillo, N. and E.A. Ceccarelli, *Open questions in ferredoxin-NADP+ reductase catalytic mechanism.* Eur J Biochem, 2003. **270**(9): p. 1900-1915.

10. Medina, M. and C. Gomez-Moreno, *Interaction of Ferredoxin-NADP(+) Reductase with its Substrates: Optimal Interaction for Efficient Electron Transfer.* Photosynth Res, 2004. **79**(2): p. 113-131.

11. Dudley, K.H., et al., *Spektren und Strukturen der am Flavin-Redoxsystem beteiligten Partikeln.* Helv. Chim. Acta, 1964. **47**: p. 1354-1383.

12. Rypniewski, W.R., et al., *Crystallization and structure determination of 2.5-.ANG. resolution of the oxidized iron-sulfur [2Fe-2S] ferredoxin isolated from Anabaena 7120.* Biochemistry, 1991. **30**(17): p. 4126–4131.

13. Morales, R., et al., *Refined X-ray Structures of the Oxidized, at 1.3 Å, and Reduced, at 1.17 Å, [2Fe−2S] Ferredoxin from the Cyanobacterium Anabaena PCC7119 Show Redox-Linked Conformational Changes. .* Biochemistry, 1999. **38**(48): p. 15764–15773.

14. Bottin, H. and B. Lagoutte, *Ferredoxin and flavodoxin from the cyanobacterium Synechocystis sp PCC 6803.* Biochim Biophys Acta, 1992. **1101**: p. 48-56.

15. Medina, M., *Structural and mechanistic aspects of flavoproteins: photosynthetic electron transfer from photosystem I to NADP+.* FEBS J., 2009. **276**: p. 3942-3958.

16. Martinez-Julvez, M., M. Medina, and C. Gomez-Moreno, *Ferredoxin-NADP(+) reductase uses the same site for the interaction with ferredoxin and flavodoxin.* J Biol Inorg Chem, 1999. **4**(5): p. 568-78.

17. Weber-Main, A.M., et al., *An Electrochemical, Kinetic, and Spectroscopic Characterization of [2Fe–2S] Vegetative and Heterocyst Ferredoxins fromAnabaena7120 with Mutations in the Cluster Binding Loop.* Archives of Biochemistry and Biophysics, 1998. **355**(2): p. 181-188.

18. Medina, M., et al., *Involvement of Glutamic Acid 301 in the Catalytic Mechanism of Ferredoxin-NADP+ Reductase from Anabaena PCC 7119.* Biochemistry, 1998. **37**(9): p. 2715-2728.

19. Nogués, I., et al., *Role of Hydrophobic Interactions in the Flavodoxin Mediated Electron Transfer from Photosystem I to Ferredoxin-NADP+ Reductase in Anabaena PCC 7119†.* Biochemistry, 2003. **42**(7): p. 2036-2045.

20. Velazquez-Campoy, A., et al., *Exact Analysis of Heterotropic Interactions in Proteins: Characterization of Cooperative Ligand Binding by Isothermal Titration Calorimetry.* Biophysical Journal, 2006. **91**(5): p. 1887-1904.

21. Martinez-Julvez, M., et al., *Lys75 of Anabaena ferredoxin-NADP+ reductase is a critical residue for binding ferredoxin and flavodoxin during electron transfer.* Biochemistry, 1998. **37**(39): p. 13604-13.

22. Martinez-Julvez, M., et al., *Role of Arg100 and Arg264 from Anabaena PCC 7119 ferredoxin-NADP+ reductase for optimal NADP+ binding and electron transfer.* Biochemistry, 1998. **37**(51): p. 17680-91.

23. Hurley, J.K., et al., *Structure-function relationships in Anabaena ferredoxin/ferredoxin:NADP(+) reductase electron transfer: insights from site-directed mutagenesis, transient absorption spectroscopy and X-ray crystallography.* Biochim Biophys Acta, 2002. **1554**(1-2): p. 5-21.

24. Goñi, G., et al., *Flavodoxin: a compromise between efficiency and versatility in the electron transfer from Photosystem I to Ferredoxin-NADP(+) reductase.* Biochim Biophys Acta, 2009. **1787**: p. 144-154.

25. Hurley, J.K., et al., *Electrostatic forces involved in orienting Anabaena ferredoxin during binding to Anabaena ferredoxin:NADP+ reductase: site-specific mutagenesis, transient kinetic measurements, and electrostatic surface potentials.* Protein Sci, 1999. **8**(8): p. 1614-22.

26. Hurley, J.K., et al., *Structure−Function Relationships in Anabaena Ferredoxin:*

Correlations between X-ray Crystal Structures, Reduction Potentials, and Rate Constants of Electron Transfer to Ferredoxin:NADP+ Reductase for Site-Specific Ferredoxin Mutants. Biochemistry, 1997. **36**(37): p. 11100-11117.

27. Hurley, J.K., et al., *Further Characterization by Site-Directed Mutagenesis of the Protein-Protein Interface in the Ferredoxin/Ferredoxin:NADP+ Reductase System from Anabaena: Requirement of a Negative Charge at Position 94 in Ferredoxin for Rapid Electron Transfer.* Archives of Biochemistry and Biophysics, 1994. **312**(2): p. 480-486.

28. Hurley, J.K., et al., *Amino acid residues in Anabaena ferredoxin crucial to interaction with ferredoxin-NADP+ reductase: Site-directed mutagenesis and laser flash photolysis.* Biochemistry, 1993. **32**(36): p. 9346-9354.

29. Hurley, J.K., et al., *An aromatic amino acid is required at position 65 in Anabaena ferredoxin for rapid electron transfer to ferredoxin:NADP+ reductase.* Journal of the American Chemical Society, 1993. **115**(25): p. 11698-11701.

30. Goñi, G., et al., *Flavodoxin-Mediated Electron Transfer from Photosystem I to Ferredoxin-NADP+ Reductase in Anabaena: Role of Flavodoxin Hydrophobic Residues in Protein−Protein Interactions†.* Biochemistry, 2008. **47**(4): p. 1207-1217.

31. Aliverti, A., M.E. Corrado, and G. Zanetti, *Involvement of lysine-88 of spinach ferredoxin-NADP+ reductase in the interaction with ferredoxin.* FEBS Lett, 1994. **343**(3): p. 247-50.

32. Landis, C.R., K.A. Rosaaen, and D.R. Sillars, *Direct observation of insertion events at rac-(C2H4(1-indenyl)2)Zr(MeB(C6F5)3)-polymeryl intermediates: distinction between continuous and intermittent propagation modes.* J Am Chem Soc, 2003. **125**(7): p. 1710-1.

33. Morales, R., et al., *A redox-dependent interaction between two electron-transfer partners involved in photosynthesis.* EMBO Reports, 2000. **1**(3): p. 271-276.

34. Kurisu, G., et al., *Structure of the electron transfer complex between ferredoxin and ferredoxin-NADP+ reductase.* Nat Struct Mol Biol, 2001. **8**(2): p. 117-121.

35. Mayoral, T., et al., *Structural analysis of interactions for complex formation between Ferredoxin-NADP+ reductase and its protein partners.* Proteins: Structure, Function, and Bioinformatics, 2005. **59**(3): p. 592-602.

36. Morales, R., et al., *Crystallographic studies of the interaction between the ferredoxin-NADP+ reductase and ferredoxin from the cyanobacterium Anabaena: looking for the elusive ferredoxin molecule.* Acta Crystallographica Section D, 2000. **56**(11): p. 1408-1412.

37. Rao, S.T., et al., *Structure of the oxidized long-chain flavodoxin from anabaena 7120 at 2 å resolution.* Protein Science, 1992. **1**(11): p. 1413-1427.

38. Hermoso, J.A., et al., *Mechanism of Coenzyme Recognition and Binding Revealed by Crystal Structure Analysis of Ferredoxin–NADP+ Reductase Complexed with NADP+.* Journal of Molecular Biology, 2002. **319**(5): p. 1133-1142.

39. Wang, M., et al., *Three-dimensional structure of NADPH–cytochrome P450 reductase: Prototype for FMN- and FAD-containing enzymes.* Proc Natl Acad Sci U. S. A, 1997. **94**(16): p. 8411–8416.

40. Madhavi Sastry, G., et al., *Protein and ligand preparation: parameters, protocols, and influence on virtual screening enrichments.* Journal of Computer-Aided Molecular Design, 2013. **27**(3): p. 221-234.

41. Basdevant, N., D. Borgis, and T. Ha-Duong, *A Coarse-Grained Protein−Protein Potential Derived from an All-Atom Force Field.* The Journal of Physical Chemistry B, 2007. **111**(31): p. 9390-9399.

42. Valdés, J.J., et al., *Tryptogalinin Is a Tick Kunitz Serine Protease Inhibitor with a Unique Intrinsic Disorder.* PLoS ONE, 2013. **8**(5): p. e62562.

43. Søndergaard, C.R., et al., *Improved Treatment of Ligands and Coupling Effects in Empirical Calculation and Rationalization of pKa Values.* Journal of Chemical Theory and Computation, 2011. **7**(7): p. 2284-2295.

44. Borrelli, K.W., et al., *PELE: Protein Energy Landscape Exploration. A Novel Monte Carlo Based Technique.* Journal of Chemical Theory and Computation, 2005. **1**(6): p. 1304-1311.

45. Madadkar-Sobhani, A. and V. Guallar, *PELE web server: atomistic study of biomolecular systems at your fingertips.* Nucleic Acids Research, 2013. **41**(W1): p. W322-W328.

46. Masone, D., et al., *H-bond network optimization in protein–protein complexes: Are all-atom force field scores enough?* Proteins: Structure, Function, and Bioinformatics, 2012. **80**(3): p. 818-824.

47. Onufriev, A., D. Bashford, and D.A. Case, *Exploring protein native states and large-scale conformational changes with a modified generalized born model.* Proteins: Structure, Function, and Bioinformatics, 2004. **55**(2): p. 383-394.

48. Zhao, Y. and D.G. Truhlar, *The M06 suite of density functionals for main group thermochemistry, thermochemical kinetics, noncovalent interactions, excited states, and transition elements: two new functionals and systematic testing of four M06-class functionals and 12 other functionals.* Theoretical Chemistry Accounts, 2008. **120**(1-3): p. 215-241.

49. Wallrapp, F., D. Masone, and V. Guallar, *Electron transfer in the P450cam/PDX complex. The QM/MM e-pathway.* J Phys Chem A, 2008. **112**(50): p. 12989-94.

50. Saen-Oon, S., M.F. Lucas, and V. Guallar, *Electron Transfer in Proteins: theory, applications and future perspectives.* Phys. Chem. Chem. Phys., 2013.

51. Voityuk, A.A. and N. Rösch, *Fragment charge difference method for estimating donor–acceptor electronic coupling: Application to DNA π-stacks* J. Chem. Phys., 2002. **117**: p. 5607-5616.

52. Voityuk, A.A., *Electron transfer between [4Fe–4S] clusters.* Chem. Phys. Lett., 2010. **495**(1-3): p. 131–134.

53. Bowers, K.J., et al. *Scalable Algorithms for Molecular Dynamics Simulations on Commodity Clusters.* in *SC 2006 Conference, Proceedings of the ACM/IEEE.* 2006.

54. Martínez-Júlvez, M., M. Medina, and A. Velázquez-Campoy, *Binding Thermodynamics of Ferredoxin:NADP(+) Reductase: Two Different Protein Substrates and One Energetics.* Biophysical Journal, 2009. **96**(12): p. 4966-4975.

55. Medina, M., et al., *Docking analysis of transient complexes: interaction of ferredoxin-NADP+ reductase with ferredoxin and flavodoxin.* Proteins, 2008. **72**(3): p. 848-62.

56. Nogués, I., et al., *Anabaena Flavodoxin as an Electron Carrier from Photosystem I to Ferredoxin-NADP+ Reductase. Role of Flavodoxin Residues in Protein−Protein Interaction and Electron Transfer†.* Biochemistry, 2005. **44**(1): p. 97-104.